COSMOLOGICAL PARAMETERS FROM THE 2003 FLIGHT OF BOOMERANG

C. J. MacTavish,[1] P. A. R. Ade,[2] J. J. Bock,[3] J. R. Bond,[4] J. Borrill,[5] A. Boscaleri,[6] P. Cabella,[7] C. R. Contaldi,[4,8]
B. P. Crill,[9] P. de Bernardis,[10] G. De Gasperis,[7] A. de Oliveira-Costa,[11] G. De Troia,[10] G. di Stefano,[12]
E. Hivon,[9] A. H. Jaffe,[8] W. C. Jones,[13] T. S. Kisner,[14] A. E. Lange,[13] A. M. Lewis,[4] S. Masi,[10]
P. D. Mauskopf,[2] A. Melchiorri,[10,15] T. E. Montroy,[14] P. Natoli,[7,16] C. B. Netterfield,[1,17]
E. Pascale,[1] F. Piacentini,[10] D. Pogosyan,[4,18] G. Polenta,[10] S. Prunet,[19] S. Ricciardi,[10]
G. Romeo,[12] J. E. Ruhl,[14] P. Santini,[10] M. Tegmark,[11]
M. Veneziani,[10] AND N. Vittorio[7,16]

ABSTRACT

We present the cosmological parameters from the CMB intensity and polarization power spectra of the 2003 Antarctic flight of the BOOMERANG telescope. The BOOMERANG data alone constrain the parameters of the ΛCDM model remarkably well and are consistent with constraints from a multiexperiment combined CMB data set. We add LSS data from the 2dF and SDSS redshift surveys to the combined CMB data set and test several extensions to the standard model including running of the spectral index, curvature, tensor modes, the effect of massive neutrinos, and an effective equation of state for dark energy. We also include an analysis of constraints to a model that allows a CDM isocurvature admixture.

Subject headings: cosmic microwave background — cosmological parameters — polarization

Online material: color figures

1. INTRODUCTION

The angular power spectra of the cosmic microwave background (CMB) have become invaluable observables for constraining cosmological models. The position and amplitude of the peaks and dips of the CMB spectra are sensitive to such parameters as the geometry of the universe, the cosmological constant, and the energy densities associated with baryons and cold dark matter (CDM) (Bond et al. 1997). The CMB intensity spectrum has been measured with high precision on large angular scales ($l < 600$) by the *Wilkinson Microwave Anisotropy Probe*

(*WMAP*) experiment (Hinshaw et al. 2003), while smaller angular scales have been probed by ground-and balloon-based CMB experiments (Ruhl et al. 2003; Readhead et al. 2004a; Dickinson et al. 2004; Kuo et al. 2004; Halverson et al. 2002). These data are broadly consistent with a ΛCDM model in which the universe is spatially flat and is composed of radiation, baryons, neutrinos, and the ever mysterious duo, CDM and dark energy.

One of the firm predictions of this *standard model* is that the CMB is intrinsically polarized. Observations of the polarization power spectra and the correlation with the total intensity spectra can therefore be used as a powerful consistency check, as well as potentially providing additional cosmological information. On large angular scales the polarization is sensitive to the details of the reionization history, and the curl component is a unique signature of tensor perturbations. On smaller angular scales the polarization spectra can verify some of the basic assumptions made in the standard model. For instance, peaks in the polarization spectra arise from the same acoustic oscillations at last scattering as those in the total intensity spectra. However, the peaks in the polarization spectra are predicted to be out of phase with the intensity peaks since the former are sourced by the velocity term of the photon-baryon fluid as opposed to its density. This effect provides the strongest constraint on the origin of the structure observed in the spectra and breaks the severe degeneracy that is introduced in models with radically broken scale invariance. These are models in which nontrivial structure may already exist in the spectrum of initial perturbations.

The recent polarization measurements of the Degree Angular Scale Interferometer (DASI) (Kovac et al. 2002), CAPMAP (Hedman et al. 2002), *WMAP* (Kogut et al. 2003), and Cosmic Background Imager (CBI) (Readhead et al. 2004b) experiments have confirmed that the CMB is indeed polarized, providing an independent means for testing the underlying model. Many of the standard model cosmological parameters are becoming highly constrained, especially in combination with complementary data sets (e.g., Seljak et al. 2004).

[1] Department of Physics, University of Toronto, 60 St. George St., Toronto, ON M5S 1A7, Canada.

[2] School of Physics and Astronomy, Cardiff University, Cardiff CF24 3YB, Wales, UK.

[3] Jet Propulsion Laboratory, Pasadena, CA. 91109.

[4] Canadian Institute for Theoretical Astrophysics, University of Toronto, Toronto, ON M5S 3H8, Canada.

[5] National Energy Research Scientific Computing Center, Lawrence Berkeley National Laboratory, Berkeley, CA 94720.

[6] IFAC-CNR, 50127 Florence, Italy.

[7] Dipartimento di Fisica, Università di Roma Tor Vergata, 00133 Rome, Italy.

[8] Department of Physics, Imperial College, London SW7 2BW, UK.

[9] Infrared Processing and Analysis Center, California Institute of Technology, Pasadena, CA 91125.

[10] Dipartimento di Fisica, Università di Roma La Sapienza, 00185 Rome, Italy.

[11] Department of Physics, Massachusetts Institute of Technology, Cambridge, MA 02139.

[12] Istituto Nazionale di Geofisica e Vulcanologia, 00143 Rome, Italy.

[13] Department of Physics, California Institute of Technology, Pasadena, CA 91125.

[14] Department of Physics, Case Western Reserve University, Cleveland, OH 44106.

[15] INFN, Sezione di Roma 1, 00133 Rome, Italy.

[16] INFN, Sezione di Roma 2, 00133 Rome, Italy.

[17] Department of Astronomy and Astrophysics, University of Toronto, Toronto, ON M5S 3H8, Canada.

[18] Department of Physics, University of Alberta, Edmonton, AB T6G 2J1, Canada.

[19] Institute d'Astrophysique de Paris, 75014 Paris, France.

In this paper we test the standard model against the data from the 2003 long-duration balloon (LDB) flight of the BOOMERANG experiment (hereafter B03). This mission marks the instrument's second successful trip over the Antarctic continent. The first LDB flight in 1998 December (hereafter B98), resulted in landmark, high signal-to-noise ratio maps of the CMB intensity anisotropy and the detection of the first few peaks of the intensity angular power spectrum (de Bernardis et al. 2000; Netterfield et al. 2002; Ruhl et al. 2003). For the 2003 flight the instrument was redesigned to be polarization sensitive, and the pointing system was upgraded to enable better attitude reconstruction. The B03 sky coverage is comprised of $\sim$195 hr of data over $\sim$1.8% of the sky, with an effective beam $11.'5 \pm 0.'23$. Instrument calibration is based on the 90 and 60 GHz *WMAP* data, and the resulting amplitude uncertainty in calibration is $\sim$2%. A complete instrument description, and the B03 CMB and Galactic maps are given in Masi et al. (2005). The final data set from the flight is comprised of four power spectra: the intensity power spectrum, TT; the EE (curl-free) and BB (curllike) polarization power spectra; and the TE cross-power spectrum. These spectral data are presented in Jones et al. (2006a), Montroy et al. (2006), and Piacentini et al. (2006).

This analysis examines in detail the cosmological implications of the B03 data set. We begin by outlining our required data products and methodology in § 2. We describe in § 3 the various data combinations that are used in this analysis. In § 4.1 we focus on the standard ΛCDM model and, applying only weakly restrictive priors, we find that the simple parameter fits to B03 data alone are fully consistent with those derived from other existing CMB data. To this CMB data, including the B03 data, we add in recent large-scale structure (LSS) redshift survey data, consisting of matter power spectra from the Sloan Digital Sky Survey (SDSS) (Tegmark et al. 2004) and the Two Degree Field Galaxy Redshift Survey (2dFGRS) (Percival et al. 2001), and determine the marginalized parameter constraints from this combined cosmological data set. In § 4.2 we extend our analysis to include tests of several modifications of the standard model with the combined data sets.

All of the models in § 4 share the assumption that the initial perturbations of the primordial plasma are adiabatic: in the early radiation-dominated era the matter and radiation densities are all identically perturbed, giving a perturbation in overall total density and hence in curvature. This is not, however, the only possibility. Isocurvature modes describe the other linear combinations of matter and radiation perturbations that do not contribute a curvature perturbation initially. Models with isocurvature contributions to the perturbations give rise to distinct signatures in the total intensity and polarization spectra. The latter can be used to further constrain the possible contributions by isocurvature modes that are not ruled out by measurements of the total intensity spectrum alone. In § 5 we explore the constraints of the B03 and other data on a model with a mixture of a dominant adiabatic mode and a subdominant isocurvature mode.

2. DATA PRODUCTS AND METHODOLOGY

2.1. *Summary of B03 Results*

We have developed two parallel and independent pipelines that we use to reduce the B03 observations from the time-ordered data to polarization and intensity anisotropy maps, through to angular power spectra. One pipeline was developed predominantly in North America (NA pipeline; C. Contaldi et al. 2006, in preparation; Jones et al. 2006b) and the other predominantly in Italy (IT pipeline; Masi et al. 2005). The purpose of constructing two separate end-to-end pipelines is to check for self-consistency at various stages during the reduction and to check for robustness

in the final spectra. We have carried out an extensive comparison of the output of the NA and IT pipelines. We find excellent agreement for both the TT spectrum (Jones et al. 2006a), representing the high signal-to-noise ratio limit, and the polarization spectra (Montroy et al. 2006; Piacentini et al. 2006), which are the most sensitive to the treatment of the experiment's noise characteristics and systematics. B03 spectra obtained from the IT pipeline were tested with the same weak priors for the standard model case. The resulting parameter determinations are in good agreement with those reported here.

The parameter constraints presented in this analysis are based on the output of the Xfaster hybrid Monte Carlo maximum likelihood estimator (C. Contaldi et al. 2006, in preparation).[20] The estimator uses a close to optimal, quadratic, Fisher matrix–based estimator that is calibrated using signal- and noise-only simulations of the entire data set, from time stream to final maps. It determines true polarization and total intensity angular power spectra (averaged over predetermined l-bands) on the sky. After an arbitrary initial guess, the quadratic estimator iterates onto the maximum likelihood solution (Bond et al. 2000), C_B^{dat}, with errors determined by an estimate of the Fisher matrix for all band powers self-consistently. This ensures that the variance for each band power includes contributions from all cross-terms and from all spectra. This is particularly important in the case of the cross-spectra, as, for example, with the TE sample variance, which is susceptible to the TT and EE power in addition to the TE power itself.

The calculation of the full Fisher matrix also allows us to exclude band powers self-consistently by cutting rows and columns from the inverse Fisher matrix. The effect of reduced sky coverage and/or pixel weighting is accounted for by computing all coupling kernels following Hivon et al. (2002) and Chon et al. (2004). The analysis typically includes a simultaneous determination of a complete set of TT, EE, BB, TE, TB, and EB band powers. The EB and TB spectra are consistent with zero (as expected) and are excluded from the parameter determination by cutting out the bands in the inverse Fisher matrix (equivalent to marginalizing over their contribution).

The spectra used in this analysis are shown in Figure 1. The data have been divided into bands that are generally $\Delta l = 50$ wide for TT and $\Delta l = 100$ wide for the three remaining spectra. The multipole ranges for the B03 spectra that are used in this analysis are presented in Table 1. All band-to-band correlations are included in the Fisher information matrix and are at most $\sim$20%. The band spacing was chosen in part to ensure that these correlations were not large.

The Xfaster code also calculates the required band window functions, W_l^B, which are used to convert the model power spectra, C_l^{mod}, into theoretical band powers via

$$\langle C_B^{\mathrm{mod}} \rangle = \frac{\mathcal{I}\left(W_l^B \mathcal{C}_l^{\mathrm{mod}}\right)}{\mathcal{I}\left(W_l^B\right)}. \qquad (1)$$

Here $\mathcal{C}_l^{\mathrm{mod}} = l(l+1)C_l^{\mathrm{mod}}/2\pi$, and we have introduced the notation for the "logarithmic integral" of a spectrum (Bond et al. 2000), $\mathcal{I}(f_l) \equiv \sum_l \{(l+1/2)/[l(l+1)]\} f_l$. The above operation permits direct comparison of theory C_B^{mod} with data C_B^{dat}.

A final issue is the potential bias introduced by the non-Gaussian distribution of the band powers in the signal-dominated regime. It has been shown (Bond et al. 2000) that the variable $Z_B = \ln(C_B^{\mathrm{dat}} + C_B^N)$ is more normally distributed than the band powers C_B. The noise offsets, C_B^N, are a measure of the deconvolved

---

[20] See http://cmb.phys.cwru.edu/boomerang and http://oberon.roma1.infn.it/boomerang/b2k.
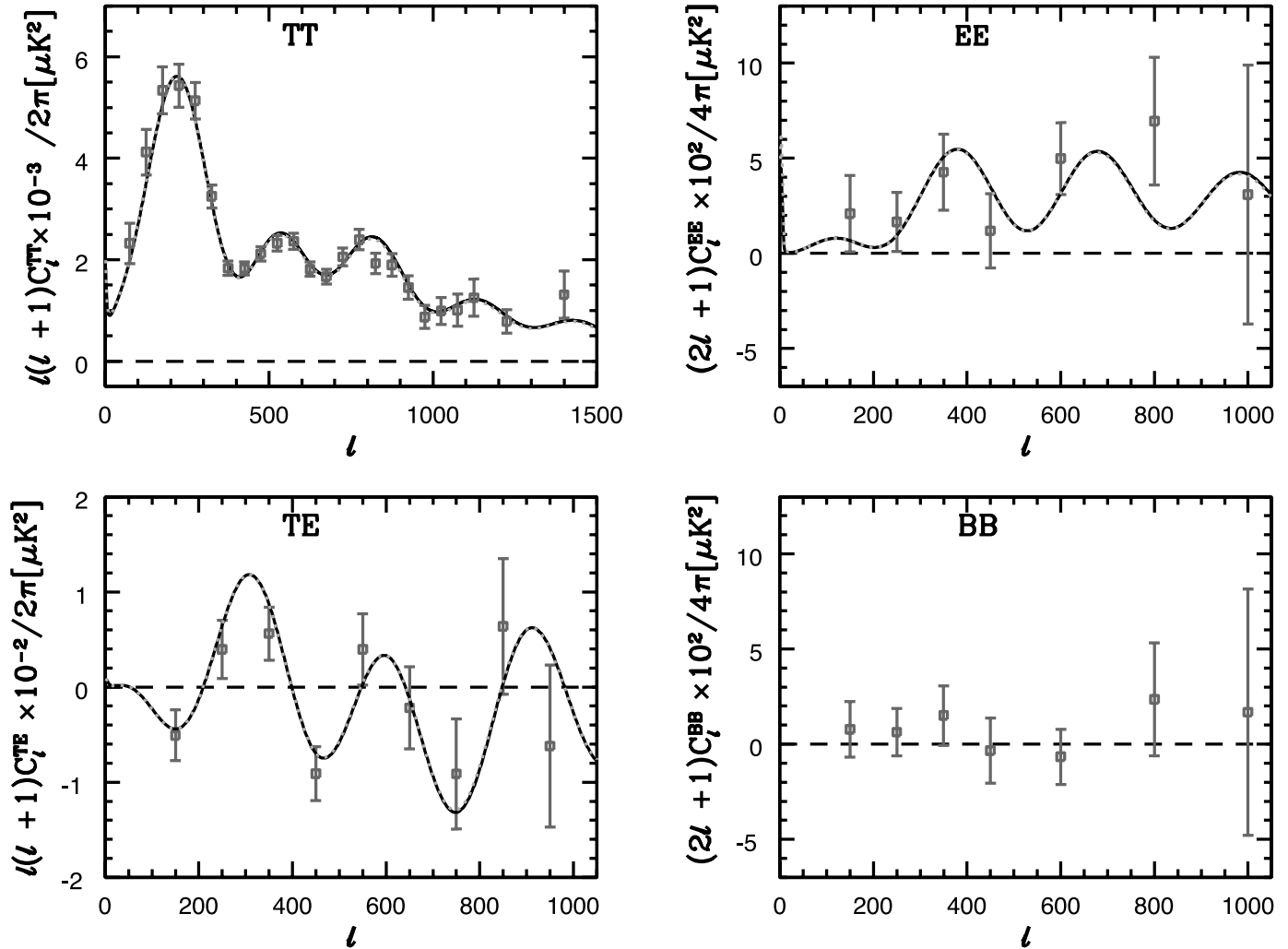
Fig. 1.—B03 band powers used in this analysis. We have included the total intensity TT, polarization EE and BB, and cross-correlation TE spectra. The EB and TB spectra are excluded from this parameter analysis. The solid curve is the previous concordance model, a best fit to *WMAP*(first-year)+CBI+ACBAR data from http://lambda.gsfc.nasa.gov/product/map/, with $[\Omega_b h^2, \Omega_c h^2, n_s(k = 0.05), \exp(-2\tau), A(k = 0.05), h] = (0.0224, 0.111, 0.958, 0.802, 0.739, 0.720)$. The dotted curve is the CMBall (Table 2)+B03 maximum likelihood ΛCDM model from this analysis with (slightly different parameterization; see text), $\{\Omega_b h^2, \Omega_c h^2, n_s(k = 0.05), \tau, \ln[10^{10} A_s(k = 0.05)], \theta\} = (0.0228, 0.108, 0.959, 0.138, 3.12, 1.04)$. [*See the electronic edition of the Journal for a color version of this figure.*]

noise spectrum on the sky and are calculated with the same quadratic estimator using Xfaster on the average of simulated noise-only observations.

The distribution of the band powers tends to a Gaussian in the noise-dominated regime and lognormal in the sample variance–dominated regime. Both limits are significant for the TT band powers; hence, we transform all the TT bands to offset lognormal variables and treat the likelihood function in the new variables as Gaussian for parameter estimation. For the polarization spectra EE and BB, which are noise-dominated, we use $Z_B = C_B^{\mathrm{dat}}$, with

TABLE 1
B03 Band Powers

B03 Spectrum	Multipole Range	Number of Bands	Reference
TT....................	$75 (375) \leq l \leq 1400$	24 (18)	Jones et al. (2006a)
TE....................	$150 \leq l \leq 950$	9	Piacentini et al. (2006)
EE and BB.......	$150 \leq l \leq 1000$	7	Montroy et al. (2006)

Notes.—The lowest band powers of the TT spectrum ($l < 375$) are excluded when combining the B03 data with the *WMAP* results since the two spectra are signal dominated and therefore correlated.

no non-Gaussian correction. For TE we also use $Z_B = C_B^{\mathrm{dat}}$ since negative values of C_B^{dat} occur. The Fisher matrix of the band powers is transformed as $\tilde{F}_{BB'} = Z_B' F_{BB'} Z_{B'}'$ with $Z_B' \equiv dZ_B/dC_B^{\mathrm{dat}} = (C_B^{\mathrm{dat}} + C_B^N)^{-1}$ if B is a TT band power and $Z_B' = 1$ otherwise. In summary, the Xfaster data products include the band powers, Fisher matrix, window functions, and noise offsets.

2.2. *Parameter Estimation Methodology*

The Monte Carlo Markov chain (MCMC) sampling technique we use for parameter estimation is described in detail in Neal (1993), Christensen et al. (2001), and Lewis & Bridle (2002) and implemented in the publicly available CosmoMC[21] package. Here we give a brief summary of the relevant details. The technique uses a Bayesian approach, generating samples of the posterior probability density function (PDF) of the parameters $\mathbf{y}$ given the data $\mathbf{z}$:

$$P(\mathbf{y}|\mathbf{z}) \propto P(\mathbf{y})P(\mathbf{z}|\mathbf{y}), \qquad (2)$$

where $P(\mathbf{z}|\mathbf{y})$ is the likelihood PDF and $P(\mathbf{y})$ is the prior PDF of $\mathbf{y}$. The posterior is sampled by running a number of Markov chains. The chains are constructed via the Metropolis-Hastings

---

[21] See http://cosmologist.info/cosmomc.

(MH) algorithm whereby a candidate parameter vector, y', is determined from an arbitrary *proposal density* distribution $q(y'|y_n)$, where y_n is the current state of the chain. The candidate y' is accepted with *acceptance probability* given by

$$\alpha(y|y_n) = \min\left[\frac{P(y'|z)q(y_n|y')}{P(y_n|z)q(y'|y_n)}, 1\right]. \quad (3)$$

At each point in the chain the acceptance probability for a candidate point is compared to a random number u drawn uniformly in the 0–1 range. If $u \le \alpha(y'|y_n)$, then the proposed vector is accepted and the next point in the chain is $y_{n+1} = y'$. If $u > \alpha(y'|y_n)$, then the proposed vector is rejected and $y_{n+1} = y_n$.

For the B03 CMB data the likelihood evaluation at each point in the chain requires the calculation of

$$\chi^2 = \sum_{BB'}\left[Z_B^{mod}(y) - Z_B^{dat}\right]\tilde{F}_{BB'}\left[Z_{B'}^{mod}(y) - Z_{B'}^{dat}\right]. \quad (4)$$

The *WMAP* data likelihood is computed using the likelihood code supplied by the *WMAP* team (Verde et al. 2003; Kogut et al. 2003), but with two modifications. The first modification is a change to the TE likelihood function to account for the correlation between the intensity and TE power spectrum estimators (we neglect the small correlations between the C_l estimators at different l) (Dore et al. 2004). After the chains have been run we use importance sampling (e.g., see Lewis & Bridle 2002) to correct the *WMAP* likelihood on large scales using the more computationally intensive likelihood code from Slosar et al. (2004). This *Slosar-Seljak modification* uses a more accurate calculation of the *WMAP* likelihood at low multipoles ($l \le 11$) and considers in more detail the errors associated with foreground removal.

The theoretical CMB spectra (as well as the matter power spectra) are computed using CAMB (Lewis et al. 2000), a fast parallel Boltzmann code based on CMBFAST (Seljak & Zaldarriaga 1996). We calculate statistics of interest, such as the marginalized posterior distribution of individual parameters, from the MCMC samples after removing burn-in. We run six chains for each combination of data and parameters that cannot be importance sampled. We marginalize numerically over each data point's calibration and beam uncertainties at each sample in the chain. The calibration errors are assumed to be independent between data sets. We check convergence by ensuring that the standard deviation between chains of the 95th percentile estimated from each chain is less than 0.2 in units of the all-chain parameter standard deviation. This should ensure that sampling errors on quoted limits are minimal.

Parameter estimates from MCMC have been shown to be in very good agreement with those derived using an adaptive C_l-grid (Bond et al. 2003) that was previously applied to the B98 analysis (Ruhl et al. 2003). MCMC results for CMBall+B98 (Bond et al. 2004) are also in good agreement with those we obtain for CMBall+B03 for the baseline model defined below with the same priors applied.[22]

3. DATA COMBINATIONS

3.1. *The CMB Data*

We consider a number of combinations of data. We break the B03 data set into one subset consisting of the TT spectrum alone (B03 TT) and into another subset consisting of the EE, BB, and TE spectra (B03 pol) alone. We also consider fits to the entire B03 data set, *WMAP* data alone, and a combined B03+*WMAP*

TABLE 2
The CMBall Data Set

Experiment	Multipole Range	Reference
WMAP TT	$2 \le l \le 899$	Hinshaw et al. (2003)
WMAP TE	$2 \le l \le 450$	Kogut et al. (2003)
DASI TT	$380 \le l \le 800$	Halverson et al. (2002)
VSA TT	$400 \le l \le 1400$	Dickinson et al. (2004)
ACBAR TT	$400 \le l \le 1950$	Kuo et al. (2004)
MAXIMA TT	$450 \le l \le 1150$	Hanany et al. (2000)
CBI TT	$750 \le l \le 1670$	Readhead et al. (2004a)

data set. We next combine B03 with available data from a collection of CMB experiments. We outline in Table 2 the experiments and multipole ranges that make up that collection, which we call CMBall. We note that because of the overlap in l range of the Archeops (Tristram et al. 2005) data with the *WMAP* data, the former cannot be included in the CMBall data set, unless a joint analysis is done. The B03 multipole range is given in Table 1. The cosmic variance of the *WMAP* and B03 data sets is correlated in the low-multipole range (essentially over the first peak of the TT power spectrum). To account for this, we cut the lower multipoles of the B03 TT spectrum ($l < 375$) when combining B03 data with *WMAP* data.

3.2. *The LSS Data*

For our final data combination we also include LSS observations from 2dFGRS and the SDSS. The two redshift surveys are treated in a conservative fashion. For example, although the SDSS band powers have been corrected for differing galaxy bias factors associated with different types of galaxies, there is still an overall galaxy bias factor, b_g, the ratio of the square root of the galaxy-galaxy power spectrum for L_* galaxies to that of the mass density power spectrum today. Although the indications are that this is a number near unity (Percival et al. 2001; Tegmark et al. 2004), in our standard results we allow it to take on arbitrary values by marginalizing it over a very broad distribution. This means that our LSS information is only constraining models through the shape of the power spectrum, but not the overall amplitude. Constraining the overall amplitude is akin to imposing a prior on σ_8. To test sensitivity to this, we have adopted varied Gaussian errors on b_g^2 about a mean. We have taken the mean to be unity and adopted errors on δb_g^2 appropriate for $\delta b_g = 0$, 0.1, 0.5, and 10, then marginalized over b_g^2. A uniform prior in b_g^2 leads to the same results as for $\delta b_g = 10$.[23] Most parameter averages we obtain are relatively insensitive to δb_g. We comment on its effect below: it has impact on the massive neutrino and dark energy equation-of-state constraints. We only use SDSS data for wavenumbers $k < 0.1\ h\ \mathrm{Mpc}^{-1}$ to avoid nonlinear corrections and to avoid possible nonuniform b_g complications. (See Tegmark et al. [2004] for a discussion of these and other issues.) A similar δb_g marginalization strategy was used for the 2dFGRS redshift survey data.

An estimate using galaxy-galaxy lensing from SDSS (Seljak et al. 2005) is $b_g = 0.99 \pm 0.07$. (These authors also used *WMAP* data to obtain this value, so it is not a completely independent determination of the bias.) An estimate using the three-point function and redshift-space clustering distortions for 2dFGRS gives $b_g = 1.04 \pm 0.04$ (Verde et al. 2002). Based on these two analyses, adopting $b_g = 1.0 \pm 0.10$ to illustrate the effect of knowing the bias better, which translates into a σ_8 prior, seems reasonable.

---

[22] B03 and B98, with overlapping sky coverage, are correlated data sets. We therefore exclude B98 from this analysis and will consider the combined B98 and B03 maps in a future analysis.

[23] Note that allowing b_g^2 to be negative has no effect and yields the same results as a (uniform) positive b_g^2 constraint.

TABLE 3
List of Weak Priors Imposed on Baseline Parameter Set

Parameter	Limits	Parameter	Limits
$\Omega_b h^2$	0.005–0.1	n_s	0.5–1.5
$\Omega_c h^2$	0.01–0.99	$\ln(10^{10}A_s)$	2.7–4.0
θ	0.5–10.0	Age (Gyr)	10–20
τ	0.01–0.8	H_0	45–90

Note.—Priors are uniform in the variable shown.

For the purposes of this paper, in which our focus is on the B03 CMB data, we have limited the LSS information we include. For example, we have not incorporated the SDSS results on luminous red galaxies (Eisenstein et al. 2005). The recent final power spectrum and window functions of the 2dFGRS survey (Cole et al. 2005) is not yet available.

3.3. Other Data Sets

We have applied the supernova data (SNe Ia) in § 4.2.5 to determine the dark energy equation of state. For this we use the *gold* set, as described in Riess et al. (2004). Also, for a few cases we include the H_0 prior value from the *Hubble Space Telescope* (*HST*) Key Project (Freedman et al. 2001).

We do not explicitly include weak-lensing results. These generally determine the parameter combination $\sigma_8 \Omega_m^{0.8}$, providing additional independent constraints (Contaldi et al. 2003; Bond et al. 2005; Readhead et al. 2004b). We also do not include information on the Lyα forest, even though it probes the power spectrum to smaller scales. Although adding this data does result in some more stringent constraints than those we derive here (McDonald et al. 2006), the forest information is more susceptible to scale-dependent biasing effects associated with gasdynamical and radiation processes.

4. ADIABATIC MODELS

4.1. Baseline Model

4.1.1. Parameterization and Priors

For our baseline model we consider a flat universe with photons, baryons, massless neutrinos, cold dark matter, and a cos-

mological constant. Initial conditions are taken to be purely adiabatic (no isocurvature modes). We assume a power-law form for the power spectrum of the primordial comoving curvature perturbation, described by $\mathcal{P}_s = A_s(k/k_\star)^{(n_s-1)}$, where n_s is the scalar spectral index and A_s is the scalar amplitude (we choose a pivot point $k_\star = 0.05$ Mpc^{-1}). The physical baryon density and dark matter density are parameterized by $\Omega_b h^2$ and $\Omega_c h^2$, respectively, where $h = H_0/100$ km s^{-1} Mpc^{-1} is the Hubble parameter. We use the parameter θ to characterize the positions of the peaks in the angular power spectra, defined as 100 times the ratio of the sound horizon to the angular diameter distance at last scattering (Kosowsky et al. 2002). Finally, the parameter τ is used to describe the Thomson scattering optical depth to decoupling. Thus, our baseline model is a function of six cosmological parameters to which we impose the following flat weak priors: $0.5 \leq n_s \leq 1.5$, $2.7 \leq \ln(10^{10}A_s) \leq 4.0$, $0.005 \leq \Omega_b h^2 \leq 0.1$, $0.01 \leq \Omega_c h^2 \leq 0.99$, $0.5 \leq \theta \leq 10.0$, and $0.01 \leq \tau \leq 0.8$. Additional weak priors restrict the age of the universe to 10 Gyr $\leq$ age $\leq$ 20 Gyr and the expansion rate to $0.45 \leq h \leq 0.9$. All priors are summarized in Table 3. Besides being generally agreed on by cosmologists, our weak priors are consistent with those used in much of the CMB literature, e.g., Lange et al. (2001), Bond et al. (2003), and Readhead et al. (2004b). We choose not to impose the restrictive prior $\tau < 0.3$ applied in Spergel et al. (2003). We note that some of our results are sensitive to our choice of prior on H_0, and we explore the effect of strengthening our H_0 prior in §§ 4.2.1 and 4.2.2.

In addition to the base parameter values, the results also include marginalized constraints for several derived parameters including Ω_Λ, the relative dark energy density; the age of the universe; Ω_m, the relative total matter density; σ_8, the rms linear mass perturbation in 8 h^{-1} Mpc spheres; z_{re}, the redshift of reionization assuming it is a sharp transition; and H_0, the Hubble constant.

4.1.2. Consistency of B03 Data Set

The resulting marginalized parameter constraints for the baseline model for each of the data combinations are given in Table 4 and presented graphically in Figure 2. In both Table 4 (and in those that follow) and Figure 2 we give the Bayesian 50% probability value (the median) obtained from the marginalized probability for each parameter. The quoted errors represent the 68%

TABLE 4
Marginalized Parameter Constraints for the Baseline, Six-Parameter, ΛCDM Model

Parameter	B03 pol	B03TT	B03	*WMAP*	*WMAP*+B03	CMBall+B03	CMBall+B03+LSS
$\Omega_b h^2$	$0.0184^{+0.0061}_{-0.0055}$	$0.0219^{+0.0031}_{-0.0030}$	$0.0217^{+0.0030}_{-0.0029}$	$0.0242^{+0.0023}_{-0.0016}$	$0.0239^{+0.0020}_{-0.0014}$	$0.0231^{+0.0014}_{-0.0010}$	$0.0226^{+0.0009}_{-0.0008}$
$\Omega_c h^2$	$0.149^{+0.053}_{-0.039}$	$0.125^{+0.034}_{-0.024}$	$0.123^{+0.034}_{-0.021}$	$0.109^{+0.017}_{-0.014}$	$0.109^{+0.014}_{-0.012}$	0.106 ± 0.010	0.120 ± 0.005
θ	1.080 ± 0.028	$1.052^{+0.009}_{-0.011}$	1.055 ± 0.010	$1.048^{+0.008}_{-0.007}$	$1.049^{+0.006}_{-0.005}$	1.045 ± 0.004	1.045 ± 0.004
τ	<0.66	<0.50	<0.49	$0.21^{+0.15}_{-0.10}$	$0.21^{+0.12}_{-0.09}$	$0.157^{+0.103}_{-0.068}$	$0.101^{+0.051}_{-0.044}$
n_s	$0.89^{+0.61}_{-0.39}$	$0.86^{+0.10}_{-0.11}$	$0.86^{+0.10}_{-0.11}$	$1.01^{+0.07}_{-0.05}$	$1.00^{+0.07}_{-0.04}$	$0.97^{+0.05}_{-0.03}$	0.95 ± 0.02
$\ln(10^{10}A_s)$	$3.4^{+0.6}_{-0.7}$	$3.4^{+0.6}_{-0.2}$	$3.3^{+0.7}_{-0.2}$	3.3 ± 0.2	3.3 ± 0.2	$3.2^{+0.2}_{-0.1}$	3.1 ± 0.1
Ω_Λ	$0.66^{+0.14}_{-0.31}$	$0.70^{+0.12}_{-0.28}$	$0.71^{+0.11}_{-0.25}$	$0.77^{+0.06}_{-0.08}$	$0.77^{+0.06}_{-0.07}$	0.77 ± 0.05	0.71 ± 0.03
Age (Gyr)	$13.0^{+1.0}_{-0.9}$	13.5 ± 0.6	$13.4^{+0.6}_{-0.5}$	$13.3^{+0.3}_{-0.4}$	$13.3^{+0.3}_{-0.4}$	$13.5^{+0.2}_{-0.3}$	13.6 ± 0.2
Ω_m	$0.34^{+0.31}_{-0.14}$	$0.30^{+0.28}_{-0.12}$	$0.29^{+0.25}_{-0.11}$	$0.23^{+0.08}_{-0.06}$	$0.23^{+0.07}_{-0.06}$	0.23 ± 0.05	0.29 ± 0.03
σ_8	1.1 ± 0.3	$0.96^{+0.19}_{-0.16}$	$0.95^{+0.20}_{-0.15}$	$0.93^{+0.13}_{-0.11}$	$0.91^{+0.09}_{-0.08}$	0.83 ± 0.06	0.84 ± 0.05
z_{re}	$33.2^{+18.6}_{-15.7}$	$23.2^{+10.6}_{-12.2}$	$22.1^{+11.2}_{-12.0}$	$19.7^{+6.6}_{-6.7}$	$19.7^{+5.3}_{-6.0}$	$16.4^{+5.4}_{-5.0}$	$12.6^{+3.9}_{-4.0}$
H_0	$70.4^{+19.6}_{-25.4}$	$69.5^{+20.5}_{-24.5}$	$71.3^{+18.7}_{-26.3}$	$75.6^{+14.4}_{-3.5}$	$75.8^{+14.2}_{-3.1}$	$75.0^{+6.4}_{-4.2}$	$69.5^{+2.5}_{-2.3}$

Notes.—Parameter uncertainties represent the 68% confidence interval obtained by integrating the marginalized distributions. The 95% confidence limits are quoted for the case of upper bounds. The following flat weak priors are imposed (as outlined in Table 3): $0.5 \leq n_s \leq 1.5$, $2.7 \leq \ln(10^{10}A_s) \leq 4.0$, $0.005 \leq \Omega_b h^2 \leq 0.1$, $0.01 \leq \Omega_c h^2 \leq 0.99$, $0.5 \leq \theta \leq 10.0$, and $0.01 \leq \tau \leq 0.8$. Additional weak priors restrict the age of the universe to 10 Gyr $\leq$ age $\leq$ 20 Gyr and the expansion rate to $45 \leq H_0 \leq 90$. The CMBall data set is as given in Table 2. The LSS data consist of the galaxy power spectra from the 2dFGRS and SDSS redshift surveys. Our baseline CMBall+B03+LSS result is fairly insensitive to δb_g, and we have chosen for this case the less restrictive, flat, uniform prior in b_g^2. The constraints from the B03 pol data are in good agreement with the B03 TT data, although some parameters constraints for the B03 pol case are prior driven, e.g., n_s, A_s, and H_0. B03 does not constrain τ, but upper limits are given. The constraints from the various data sets are consistent.
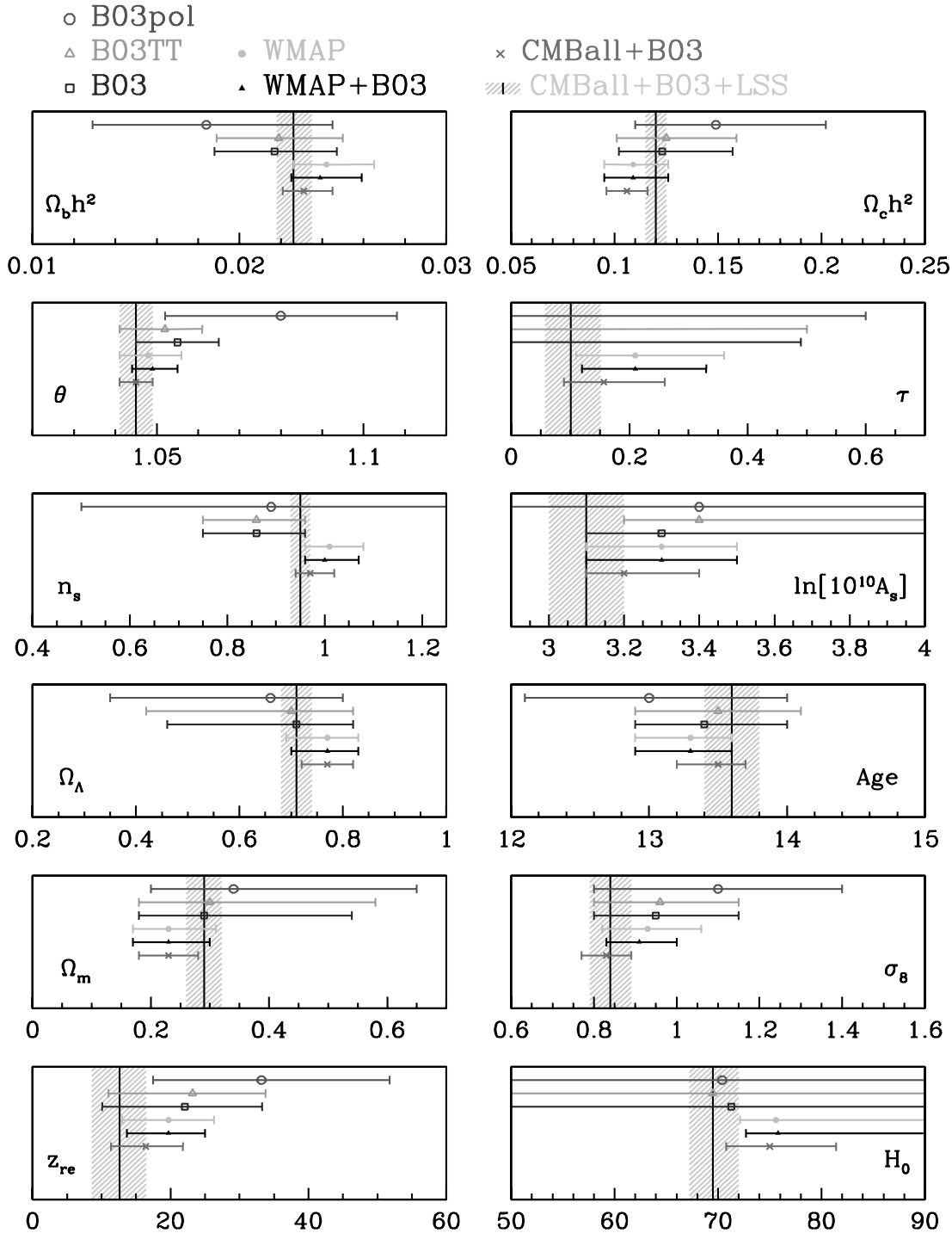
Fig. 2.—Median values obtained from the marginalized probability for each parameter for the baseline, standard model. The error bars represent the 68% confidence interval. The 95% upper limit is given for the case of τ for B03 data alone. The following flat weak priors are imposed (as outlined in Table 3): $0.5 \leq n_s \leq 1.5$, $2.7 \leq \ln(10^{10}A_s) \leq 4.0$, $0.005 \leq \Omega_b h^2 \leq 0.1$, $0.01 \leq \Omega_c h^2 \leq 0.99$, $0.5 \leq \theta \leq 10.0$, and $0.01 \leq \tau \leq 0.8$. Additional weak priors restrict the age of the universe to 10 Gyr $\leq$ age $\leq$ 20 Gyr and the expansion rate to $45 \leq H_0 \leq 90$. Our baseline CMBall+B03+LSS result is fairly insensitive to δb_g, and we have chosen for this case the less restrictive flat, uniform prior in b_g^2. [See the electronic edition of the Journal for a color version of this figure.]

confidence interval obtained by integrating the marginalized distributions. In the case of upper or lower bounds, the 95% confidence limits are quoted. We note that our baseline CMBall+B03+LSS result is fairly insensitive to δb_g and that we have chosen the less restrictive flat, uniform prior in b_g^2.

The comparison of B03 pol and B03 TT provides a robust internal consistency check. We note that the B03 pol constraints to $\Omega_b h^2$ and $\Omega_c h^2$ are quite good with uncertainties that are only slightly larger than those of the B03 TT result. However, the B03

pol constraints on n_s, τ, and A_s are weak, and results for these cases are prior-driven. We present in Figure 3 a two-dimensional likelihood plot of θ versus the combined parameter $A_s e^{-2\tau}$. The latter determines the overall power in the *observed* CMB anisotropy (except at low l) and is therefore better constrained than the primordial power A_s. CosmoMC uses a covariance matrix for the parameters and is therefore able to ascertain linear combination degeneracies. Although we use $\ln A_s$ and τ as base parameters, the proposal density knows that the combination $\ln(A_s e^{-2\tau})$
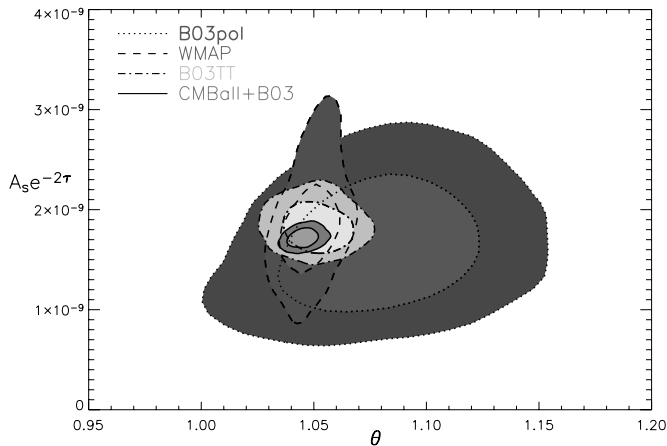
Fig. 3.—Constraints on $A_s e^{-2\tau}$ vs. θ. Inner contours represent 68% likelihood regions, and outer contours represent 95% likelihood regions. The peak position characterization parameter θ is the best-determined parameter in cosmology, 1.045 ± 0.004, from the CMBall+B03 data set. We find that the B03 TT data do particularly well at constraining both the peak pattern and the combined $A_s e^{-2\tau}$ amplitude parameter. The constraint from *WMAP* alone on A_s is better than that from B03. The agreement between the B03 pol and B03 TT data is consistent with the basic inflation picture. [*See the electronic edition of the Journal for a color version of this figure.*]

is well constrained and can explore the poorly constrained orthogonal direction efficiently. We find that the B03 data alone do particularly well at constraining $A_s e^{-2\tau}$. The angular diameter distance variable θ defines the shift with l of the overall C_l pattern, in particular, of the pattern of peaks and troughs. With all of the CMB data it is the best-determined parameter in cosmology, 1.045 ± 0.004; with B03 pol it is an important test that demonstrates the consistency of the positions of the polarization spectra peaks and troughs relative to those forecasted from the TT data, although the errors are larger with $\theta = 1.08 \pm 0.03$. For the CBI TT, TE, and EE data in combination with *WMAP* TT and TE, Readhead et al. (2004b) found $\theta = 1.044 \pm 0.005$. With just the CBI EE polarization data they determined $\theta = 1.06 \pm 0.04$, again showing the consistency we find of the data with the TT forecast of the polarization peaks and trough.

The B03 median parameter values are remarkably consistent with the parameter constraints from *WMAP* data alone. We note that in general the Slosar-Seljak modification to *WMAP* tends to broaden *WMAP* parameter likelihood curves and that the most significant impact on the median values is in τ ($\sim 0.3\,\sigma$ increase) and in Ω_m ($\sim 0.6\,\sigma$ decrease). Adding B03 to the *WMAP* data decreases the parameter uncertainties by an average of $\sim 15\%$. The most significant effect is a $\sim 30\%$ decrease in the σ_8 uncertainty. Figure 4 shows the likelihood curves for the six base parameters and six derived parameters for a variety of data combinations. Overall the various data combinations are generally in good agreement at better than the $1\,\sigma$ level. The largest outlier is $\Omega_c h^2$, which increases by $1.5\,\sigma$ with the addition of the LSS data set. Also, similar to Spergel et al. (2003), we find that the addition of small-scale CMB data lowers both the value for the amplitude of fluctuations at $k = 0.05\,\mathrm{Mpc}^{-1}$ and the value of the scalar spectral index. The effect of adding the LSS data follows this trend.

4.2. *Modified Standard Model*

In this section we explore five extensions of the standard model by adding, in turn, one parameter to the baseline parameter set. In all cases we maintain the same weak priors on the base parameters as outlined in Table 3. Some of the results are sensitive to our

chosen prior range for H_0. For example, in certain cases we note the impact of strengthening our H_0 prior to the value from the *HST* Key Project (Freedman et al. 2001), $h = 0.72 \pm 0.08$, with the errors treated as Gaussian.

4.2.1. *Running Index*

We modify the power-law form for the power spectrum of the density perturbations to allow the spectral index, n_s, to vary with scale. Following Kosowsky & Turner (1995) this variation can be parameterized by the term $n_{\mathrm{run}} = dn_s/d\ln k$, such that $n_s = n_s(k_\star) + n_{\mathrm{run}}(k_\star)\ln(k/k_\star)$, where again $k_\star = 0.05\,\mathrm{Mpc}^{-1}$. We restrict n_{run} to lie between -0.3 and 0.3. Results from the combined data sets, CMBall+B03 and CMBall+B03+LSS, are given in Table 5.

Spergel et al. (2003) report a detection of the running index of $n_{\mathrm{run}} = -0.031^{+0.016}_{-0.017}$ from their combined *WMAP*ext+2dFGRS+Lyα data set. Slosar et al. (2004) present a reduction in significance of the detection of n_{run} when their full likelihood analysis and detailed foreground removal is applied to the *WMAP* data. We find that the Slosar-Seljak modification to *WMAP* decreases the significance of n_{run} but that inclusion of the data from the small-scale CMB experiments has the opposite effect (as was found by Spergel et al. [2003]). From CMB data alone we determine a median value for $n_{\mathrm{run}} = -0.071^{+0.035}_{-0.037}$. This result is somewhat sensitive to our choice of prior. Spergel et al. (2003) apply a strong $\tau < 0.3$ prior that effectively reduces the median value of n_{run} for their CMB data–only case. Here we apply a Gaussian *HST* prior on H_0 that lowers the significance of the running index to $n_{\mathrm{run}} = -0.065 \pm 0.035$ for the CMBall+B03 data set. Inclusion of the LSS data (with uniform prior in b_g^2) further reduces the significance, and our median value from the larger combined data set is $n_{\mathrm{run}} = -0.050^{+0.026}_{-0.027}$. We note that the application of a Gaussian prior to b_g^2 has no impact on the running index parameter. Application of the *HST* prior on H_0 yields a final median value $n_{\mathrm{run}} = -0.048 \pm 0.026$ for the CMBall+B03+LSS(+*HST*) data set. Figure 5 shows the likelihood curves for the n_{run} parameter for various data combinations. It is interesting to compare our result with that of Seljak et al. (2004), who argue that if the state-of-the-art modeling of Lyα forest measurements is dominated by statistical rather than systematic errors, then $|n_{\mathrm{run}}| < 0.01$.

4.2.2. *Curvature*

We consider a modification to the standard model that allows the possibility of nonflat geometry. We parameterize the curvature density by Ω_k and allow it to vary between -0.3 and 0.3. Table 5 shows the results for the CMBall+B03 and CMBall+B03+LSS data sets. The CMB data, with Table 3 weak priors, place a constraint on the curvature that is $\Omega_k = -0.030^{+0.026}_{-0.046}$. We show in Figure 6 the likelihood profiles for *WMAP*, *WMAP*+B03, CMBall+B03, and CMBall+B03+LSS. While the addition of B03 data to the *WMAP* data tends to lower the significance of curvature, adding more small-scale CMB data increases the width of the low-end tail. Addition of the LSS data, with uniform prior in b_g^2, yields a median value of $\Omega_k = -0.024^{+0.014}_{-0.019}$. Application of the Gaussian prior in b_g^2 (with 10% uncertainty in b_g) has a slight effect with a resulting median value of $\Omega_k = -0.021^{+0.014}_{-0.016}$. If we restrict the H_0 value by the application of a Gaussian *HST* prior, the curvature density determined from the CMBall+B03 data set is $\Omega_k = -0.013^{+0.014}_{-0.018}$. Moreover, application of the more stringent H_0 prior reduces the median value of the curvature from the combined CMBall+B03+LSS data set (flat b_g^2 prior) to $\Omega_k = -0.017^{+0.011}_{-0.014}$. Our result agrees well with the constraint $\Omega_k = -0.010 \pm 0.009$ obtained by combining CMB
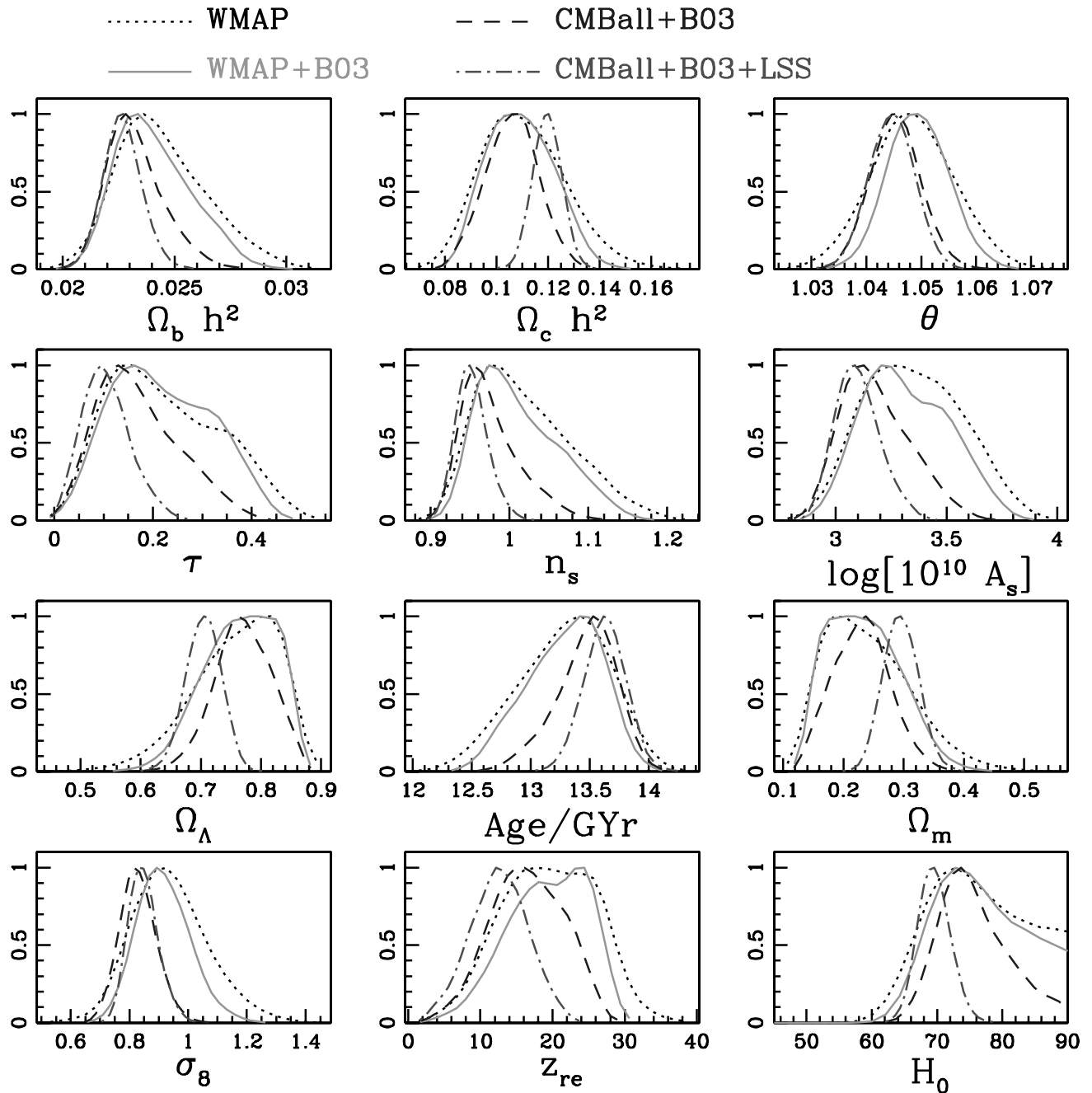
Fig. 4.—Marginalized one-dimensional distributions for the baseline model parameters for the data combinations *WMAP* only (*dotted*), *WMAP*+B03 (*solid*), CMBall+B03 (*dashed*), and CMBall+B03+LSS (*dash-dotted*). The curves are each normalized by their peak values. All distributions are derived from chains run with the weak set of external, uniform priors shown in Table 3. The LSS data consist of the 2dFGRS and SDSS redshift surveys (with a flat b_g^2 prior imposed). The most significant impact of the B03 data is on σ_8. Moreover, the σ_8 constraint from CMB data alone is quite strong, with the addition of LSS data having little effect. [*See the electronic edition of the Journal for a color version of this figure.*]

data with the red luminous galaxy clustering data, which has its own signature of baryon acoustic oscillations (Eisenstein et al. 2005).

4.2.3. *Tensor Modes*

So far we have assumed only scalar perturbations. However, inflationary models can produce tensor perturbations from gravitational waves that are predicted to evolve independently of the scalar perturbations, with an uncorrelated power spectrum $\mathcal{P}_t$. The amplitude of a tensor mode falls off rapidly after horizon crossing, and the effect is therefore predominantly on the largest scales: tensor modes entering the horizon along the line of sight to last scat-

tering distort the photon propagation and generate an additional anisotropy pattern. We parameterize the tensor component by the ratio A_t/A_s, where A_t is the primordial power in the transverse traceless part of the metric tensor on 0.05 Mpc^{-1} scales. We impose a very weak prior on the amplitude ratio, restricting it to lie between 0 and 20.

A tensor spectral index, defined by $\mathcal{P}_t \propto k^{n_t}$, must also be set. In inflation models it is related to the amplitude ratio by $A_t/A_s \approx -8n_t/(1 - n_t/2)$, so one parameter suffices. In a nearly uniformly accelerating regime, $n_t \approx n_s - 1$ is also expected. However, although $n_s > 1$ can arise in inflation models, $n_t > 0$ is difficult to

TABLE 5
MARGINALIZED PARAMETER CONSTRAINTS FOR FIVE MODIFICATIONS OF THE BASELINE MODEL

PARAMETER	BASE+RUNNING INDEX		BASE+CURVATURE		BASE+TENSOR MODES	
	CMBall +B03	CMBall+LSS+B03	CMBall+B03	CMBall+LSS+B03	CMBall+B03	CMBall+LSS+B03
$\Omega_b h^2$	$0.0237^{+0.0020}_{-0.0019}$	$0.0218^{+0.0010}_{-0.0009}$	$0.0227^{+0.0014}_{-0.0009}$	$0.0226^{+0.0010}_{-0.0009}$	0.0246 ± 0.0013	$0.0232^{+0.0010}_{-0.0009}$
$\Omega_c h^2$	$0.102^{+0.017}_{-0.011}$	0.125 ± 0.007	$0.108^{+0.009}_{-0.013}$	0.111 ± 0.008	$0.0945^{+0.0102}_{-0.0074}$	0.117 ± 0.006
θ	1.048 ± 0.005	1.044 ± 0.004	$1.044^{+0.005}_{-0.004}$	1.044 ± 0.004	$1.048^{+0.004}_{-0.005}$	1.046 ± 0.004
τ	$0.33^{+0.11}_{-0.16}$	$0.145^{+0.031}_{-0.030}$	$0.149^{+0.115}_{-0.064}$	$0.128^{+0.032}_{-0.118}$	$0.158^{+0.076}_{-0.066}$	$0.0991^{+0.0542}_{-0.0438}$
n_s	$0.96^{+0.05}_{-0.06}$	0.90 ± 0.04	$0.96^{+0.05}_{-0.02}$	$0.95^{+0.03}_{-0.02}$	$1.02^{+0.03}_{-0.04}$	$0.97^{+0.03}_{-0.02}$
$\ln(10^{10}A_s)$	$3.5^{+0.2}_{-0.3}$	3.2 ± 0.1	$3.2^{+0.2}_{-0.1}$	3.1 ± 0.1	3.1 ± 0.1	3.1 ± 0.1
Ω_Λ	$0.80^{+0.05}_{-0.09}$	0.67 ± 0.04	$0.68^{+0.11}_{-0.15}$	$0.67^{+0.04}_{-0.05}$	$0.83^{+0.03}_{-0.04}$	0.72 ± 0.03
Age (Gyr)	13.3 ± 0.4	13.7 ± 0.2	14.9 ± 1.3	$14.7^{+0.7}_{-0.6}$	$13.2^{+0.3}_{-0.2}$	13.5 ± 0.2
Ω_m	$0.20^{+0.09}_{-0.05}$	0.33 ± 0.04	$0.35^{+0.19}_{-0.13}$	$0.35^{+0.06}_{-0.05}$	$0.173^{+0.044}_{-0.026}$	$0.28^{+0.03}_{-0.03}$
σ_8	0.91 ± 0.07	$0.88^{+0.07}_{-0.05}$	$0.81^{+0.06}_{-0.05}$	$0.81^{+0.06}_{-0.05}$	0.77 ± 0.07	0.84 ± 0.05
z_{re}	$26.2^{+4.1}_{-8.0}$	16.8 ± 5.0	$16.0^{+6.3}_{-4.9}$	$14.5^{+4.9}_{-4.5}$	$15.4^{+4.3}_{-4.6}$	12.2 ± 4.0
H_0	$78.7^{+11.3}_{-9.3}$	$66.7^{+1.5}_{-1.4}$	$61.3^{+14.3}_{-16.3}$	$61.8^{+2.3}_{-2.3}$	>73.2	$71.2^{+3.1}_{-2.7}$
n_{run}	$-0.071^{+0.035}_{-0.037}$	$-0.050^{+0.026}_{-0.027}$	...	...	...	...
Ω_k	...	...	$-0.030^{+0.026}_{-0.046}$	$-0.024^{+0.014}_{-0.019}$	...	...
A_t/A_s	...	...	...	...	<0.71	<0.36
f_ν	...	...	...	...	...	...
w	...	...	...	...	...	...

PARAMETER	BASE+MASSIVE NEUTRINOS		BASE+w		BASELINE	
	CMBall+B03	CMBall+LSS+B03	CMBall+B03	CMBall+LSS+B03+SNe Ia	CMBall+B03	CMBall+LSS+B03
$\Omega_b h^2$	$0.0224^{+0.0016}_{-0.0011}$	$0.0224^{+0.0009}_{-0.0008}$	0.0234 ± 0.0013	0.0229 ± 0.0009	$0.0233^{+0.0013}_{-0.0012}$	0.0227 ± 0.0008
			$0.0232^{+0.0015}_{-0.0011}$	0.0228 ± 0.0009	$0.0231^{+0.0014}_{-0.0010}$	$0.0226^{+0.0009}_{-0.0008}$
$\Omega_c h^2$	$0.121^{+0.013}_{-0.015}$	$0.125^{+0.008}_{-0.007}$	$0.106^{+0.010}_{-0.011}$	$0.117^{+0.007}_{-0.008}$	0.106 ± 0.010	0.120 ± 0.005
θ	1.046 ± 0.005	1.045 ± 0.004	$1.046^{+0.005}_{-0.004}$	1.045 ± 0.004	1.045 ± 0.004	1.045 ± 0.004
τ	$0.145^{+0.114}_{-0.069}$	$0.103^{+0.054}_{-0.042}$	$0.150^{+0.089}_{-0.066}$	$0.110^{+0.061}_{-0.047}$	$0.157^{+0.103}_{-0.068}$	$0.101^{+0.051}_{-0.044}$
n_s	$0.94^{+0.05}_{-0.03}$	0.94 ± 0.02	$0.97^{+0.05}_{-0.03}$	$0.96^{+0.03}_{-0.02}$	$0.97^{+0.05}_{-0.03}$	0.95 ± 0.02
$\ln(10^{10}A_s)$	$3.1^{+0.2}_{-0.1}$	3.1 ± 0.1	$3.1^{+0.2}_{-0.1}$	3.1 ± 0.1	$3.2^{+0.2}_{-0.1}$	3.1 ± 0.1
Ω_Λ	$0.64^{+0.12}_{-0.11}$	$0.65^{+0.05}_{-0.06}$	$0.74^{+0.08}_{-0.13}$	0.70 ± 0.02	0.77 ± 0.05	0.71 ± 0.03
Age (Gyr)	$14.2^{+0.3}_{-0.5}$	13.9 ± 0.2	$13.6^{+0.4}_{-0.3}$	13.6 ± 0.2	$13.5^{+0.2}_{-0.3}$	13.6 ± 0.2
Ω_m	$0.36^{+0.11}_{-0.12}$	$0.35^{+0.06}_{-0.05}$	$0.26^{+0.13}_{-0.08}$	0.30 ± 0.02	0.23 ± 0.05	0.29 ± 0.03
σ_8	$0.58^{+0.15}_{-0.11}$	$0.73^{+0.08}_{-0.07}$	$0.77^{+0.14}_{-0.15}$	0.82 ± 0.06	0.83 ± 0.06	0.84 ± 0.05
z_{re}	$16.3^{+6.4}_{-5.6}$	$13.0^{+4.1}_{-3.9}$	16.0 ± 5.0	$13.3^{+4.3}_{-3.9}$	$16.4^{+5.4}_{-4.0}$	$12.6^{+3.9}_{-4.0}$
H_0	$63.1^{+9.9}_{-5.6}$	$64.9^{+3.8}_{-3.9}$	$69.9^{+13.2}_{-12.8}$	$68.5^{+2.1}_{-2.0}$	$75.0^{+6.4}_{-4.2}$	$69.5^{+2.5}_{-2.3}$
n_{run}	...	...	...	...	...	...
Ω_k	...	...	...	...	...	...
A_t/A_s	...	...	...	...	...	...
f_ν	<0.21	<0.09	...	...	...	...
w	...	...	$-0.86^{+0.35}_{-0.36}$	$-0.94^{+0.093}_{-0.097}$	...	...

NOTES.—Parameter uncertainties represent the 68% confidence interval. For the case of upper or lower bounds 95% confidence limits are quoted. The following flat weak priors are imposed on the base six parameters (as outlined in Table 3): $0.5 \leq n_s \leq 1.5$, $2.7 \leq \ln(10^{10}A_s) \leq 4.0$, $0.005 \leq \Omega_b h^2 \leq 0.1$, $0.01 \leq \Omega_c h^2 \leq 0.99$, $0.5 \leq \theta \leq 10.0$, and $0.01 \leq \tau \leq 0.8$. Additional weak priors restrict the age of the universe to 10 Gyr $\leq$ age $\leq$ 20 Gyr and the expansion rate to $45 \leq H_0 \leq 90$. We add, in turn, one parameter to the base set and impose the following prior on each: running index, $-0.3 < n_{run} < 0.3$; curvature, $-0.3 < \Omega_k < 0.3$; amplitude ratio, $0 < A_t/A_s < 20$; neutrino fraction of dark matter, $0 < f_\nu < 1$; and dark energy equation of state, $-4 < w < 0$. The CMBall data set is as given in Table 2. The LSS data consist of the matter power spectra from the 2dFGRS and SDSS redshift surveys. We have marginalized the galaxy bias factor b_g assuming a uniform flat prior in b_g^2. For the base+w case only we add in both the LSS and SNe Ia data, which gives a better constrained result than that which is obtained from adding LSS data alone. We include the baseline model results for comparison.

obtain. As well, for many inflation models with $n_s - 1$ just below zero, n_t comes out to be slightly closer to zero. If the acceleration changes significantly over the observable range, n_t and n_s would not be intimately tied. Rather than let n_t float as a second added parameter, we have chosen to make $\mathcal{P}_t$ flat in k (and thus set n_t to zero) for the computations of the tensor-induced component of $\mathcal{C}_l$.

Results are presented in Table 5, and Figure 7 illustrates the likelihood curves for the amplitude ratio for a number of data combinations. The influence of the high precision of the *WMAP* data on the largest scales is evident. Adding the small-scale CMB data only slightly reduces the limit. We determine an upper limit on the tensor ratio from CMB data (CMBall+B03 data set) alone of $A_t/A_s < 0.71$ (95% confidence limit). The CMB data appear to select models with relatively large tensor-to-scalar ratios. However, these models that have large values for the Hubble parameter ($H_0 \sim 85$) are allowed due to the poor constraint on H_0 when including tensor modes. In this case, the constraints on H_0 are driven
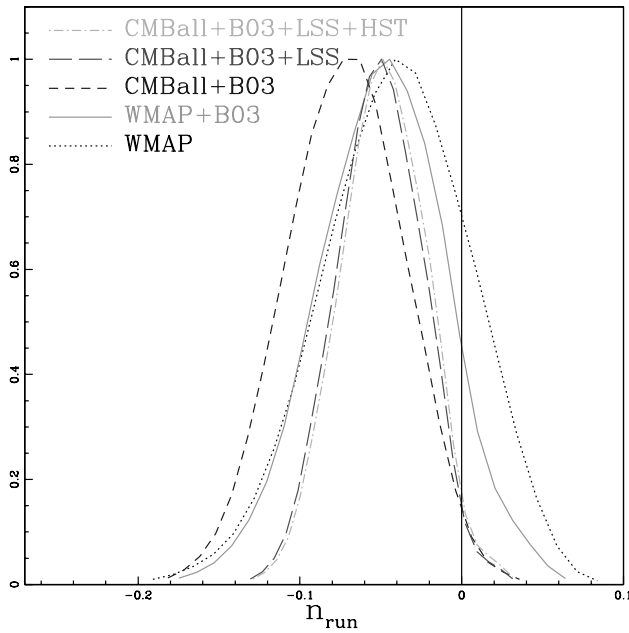
FIG. 5.—Marginalized one-dimensional distributions for the n_{run} parameter for the baseline+running index model. Weak priors imposed are those outlined in Table 3. The running index parameter is restricted to lie between -0.3 and 0.3. Application of the *HST* prior on H_0 slightly reduces the significance of a running index. [*See the electronic edition of the Journal for a color version of this figure.*]
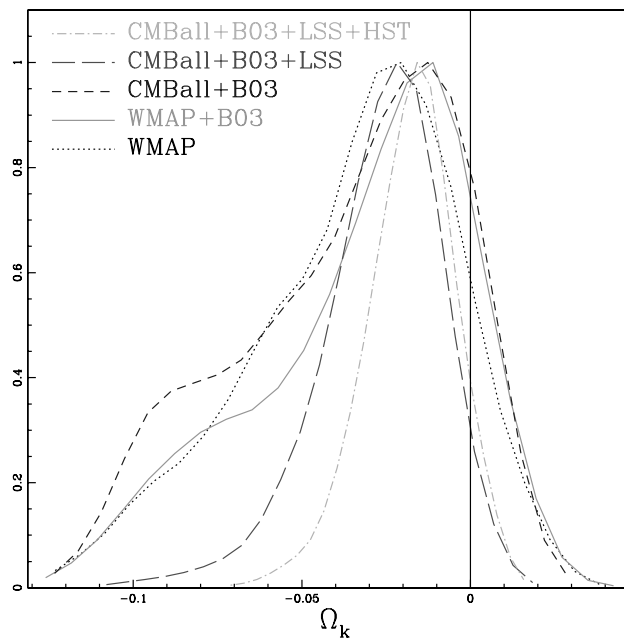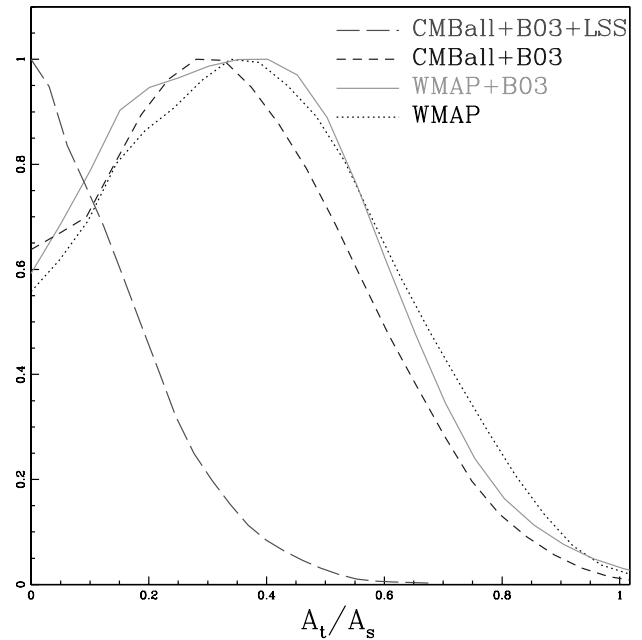

FIG. 7.—Marginalized one-dimensional distributions for the amplitude ratio A_t/A_s for the baseline model modification that allows tensor modes. Weak priors imposed are those outlined in Table 3. We impose the weak prior $0 < A_t/A_s < 20$ to the tensor contribution. We find from CMB data alone (CMBall+B03) an upper limit (95% confidence) on the amplitude ratio of $A_t/A_s < 0.71$. For these models, however, H_0 is only poorly constrained (see text). Addition of the LSS data reduces this limit to $A_t/A_s < 0.36$. [*See the electronic edition of the Journal for a color version of this figure.*]

FIG. 6.—Marginalized one-dimensional distributions for Ω_k for the baseline model that allows nonzero curvature. Weak priors imposed are those outlined in Table 3. We restrict Ω_k to the range -0.3 to 0.3. The relatively wide scope for positive curvature is associated with the angular diameter distance degeneracy, which is only partly broken by the CMB data. Application of the *HST* prior on H_0 to the larger combined data set somewhat reduces the possibility of significant curvature. [*See the electronic edition of the Journal for a color version of this figure.*]

mainly by our choice of weak priors, and the data only provide a lower limit (see Table 5). We find with application of the *HST* prior (which excludes these models with large H_0 values) that the tensor limit from the CMBall+B03 data set is reduced to $A_t/A_s < 0.635$. A similar effect is obtained with the addition of the LSS data, which further reduces the limit to $A_t/A_s < 0.36$. When we constrain b_g in the LSS data, the limits are very similar. The application of the more restrictive prior discussed above, with only $n_s \leq 1$ allowed to have a tensor contribution, lowers the CMBall+B03 limit to $A_t/A_s < 0.45$ and the CMBall+B03+LSS limit to $A_t/A_s < 0.31$. As a final case we set $n_t = -(A_t/A_s)/8$ and found $A_t/A_s < 0.54$ for the CMBall+B03 data set and $A_t/A_s < 0.30$ for the combined CMBall+B03+LSS results (again applying the b_g constraint has little effect).

4.2.4. *Massive Neutrinos*

Measurements from solar and atmospheric neutrino experiments, such as the Sudbury Neutrino Observatory (Ahmad et al. 2002) and Super-Kamiokande (Toshito et al. 2001), indicate that neutrinos change flavor: different generations of neutrinos oscillate into each other. The implication of flavor changing is that neutrinos have mass. Given that neutrinos are the second most abundant particles in the universe, massive neutrinos could have considerable impact on the energy density of the early universe. We consider here the case of three neutrinos of degenerate mass, such that $\Omega_\nu h^2 = 3m_\nu/(94.0 \text{ eV})$. This assumption is well justified given the small square mass difference measured by oscillation experiments (at most $\delta m_\nu^2 \sim 10^{-3}$ eV; Aliani et al. 2003). We parameterize the massive neutrino contribution as a fraction of the dark matter energy density, $f_\nu = \Omega_\nu h^2/\Omega_{\mathrm{DM}} h^2 = 1 - \Omega_{\mathrm{CDM}} h^2/\Omega_{\mathrm{DM}} h^2$.

Results for the combined data sets are given in Table 5. From CMB data alone the upper limit on the neutrino fraction is
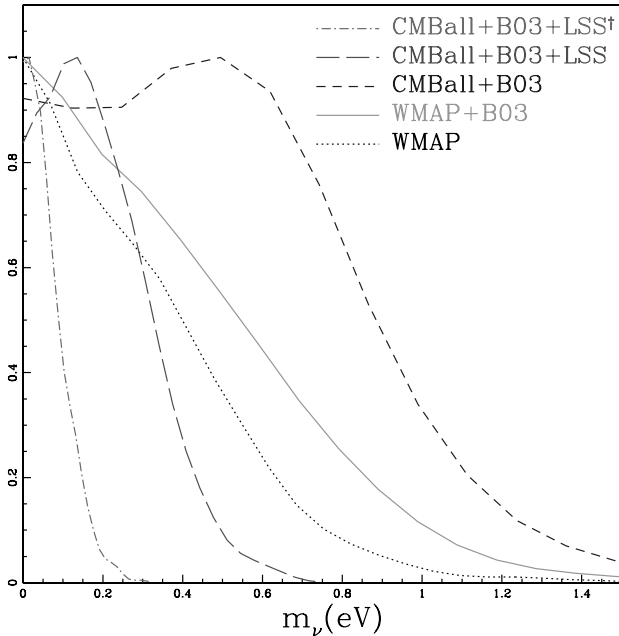
FIG. 8.—Marginalized one-dimensional distributions for m_ν for the baseline model that allows massive neutrinos (three species of degenerate mass). Weak priors imposed are those outlined in Table 3. We parameterize the massive neutrino contribution as a fraction of the dark matter energy density, $f_\nu = \Omega_\nu h^2 / \Omega_{DM} h^2$. We find from CMB data alone (CMBall+B03) an upper limit (95% confidence) on the neutrino mass of $m_\nu < 1.0$ eV. Adding the LSS data reduces this limit to $m_\nu < 0.40$ eV, without any b_g constraint, and to $m_\nu < 0.16$ eV, when $b_g = 1.0 \pm 0.10$ is used. [See the electronic edition of the Journal for a color version of this figure.]

FIG. 9.—Marginalized one-dimensional distributions for the dark matter equation-of-state parameter w. Weak priors imposed on the base parameters are those outlined in Table 3. We also impose the prior $-4 < w < 0$. The dagger denotes the application of a Gaussian prior to b_g^2 (with $b_g = 1\% \pm 10\%$). The nominal flat uniform prior on b_g^2 yields a slightly higher median value for w, driven by higher values of b_g. Adding the SNe Ia data, however, reduced the median value to $-0.94^{+0.093}_{-0.097}$. [See the electronic edition of the Journal for a color version of this figure.]

$f_\nu < 0.21$ (95% confidence limit). This translates to an upper limit on the neutrino mass of $m_\nu < 1.0$ eV, or $\Omega_\nu h^2 < 0.033$. This limit is more stringent than the 3 eV upper limit on the electron neutrino mass determined from tritium β-decay experiments and recommended in the Review of Particle Physics (Eidelman et al. 2004). Including the LSS data (flat b_g^2 prior) pushes this limit down considerably to $f_\nu < 0.093$ (95% confidence) and limits the neutrino mass to $m_\nu < 0.40$ eV. This result is somewhat larger than that found in Spergel et al. (2003). We find that addition of more and more small-scale CMB data drives the limit up, as is evident in Figure 8. When $b_g = 1.0 \pm 0.10$ is used, the neutrino fraction upper limit is reduced to $f_\nu < 0.041$ (95% confidence), corresponding to a neutrino mass limit of $m_\nu < 0.16$ eV. This neutrino mass limit is in good agreement with the strong limit ($m_\nu < 0.18$ eV) obtained by Seljak et al. (2005), who included the bias constraint and the SDSS and WMAP data. In their analysis of b_g they found $\sigma_8 = 0.85^{+0.07}_{-0.06}$, with $b_g = 1.02^{+0.08}_{-0.08}$. This compares with the values we obtain: $\sigma_8 = 0.85 \pm 0.04$, with $\delta b_g = 0.10$, and $\sigma_8 = 0.73^{+0.08}_{-0.07}$, with $\delta b_g = \infty$.

4.2.5. Dark Energy

The standard model predicts (and CMB observations strongly support) a universe that is nearly flat, implying a total energy density approaching critical. The total matter density, however, comprises only one-third of the total energy density. The prevailing energy density component comes from some form of dark energy that up to now we have assumed takes the form of a vacuum density or cosmological constant, Λ, with equation of state described by $w = p/\rho = -1$, where p and ρ are the dark energy pressure and density, respectively. We now consider the possibility that the dark energy component is a rolling scalar field or quintessence (see, e.g., Ratra & Peebles 1988 or Huey et al. 1999), allowing the effective constant equation-of-state parameter w to
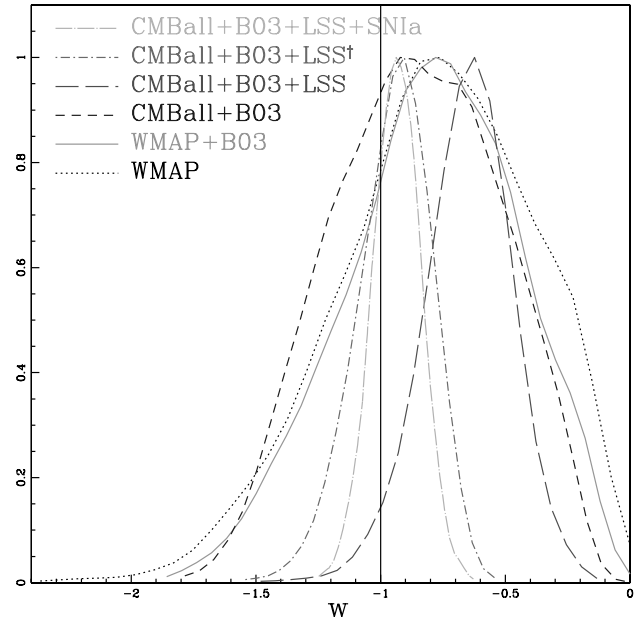
differ from -1. We treat w as a redshift-independent phenomenological factor and allow it to range with a uniform prior over the range -4 to 0. We have also run the cases with w restricted to lie in the range -1 to 0 and find similar limits. To be self-consistent, perturbations in the dark energy should be allowed for when w is not -1, although these have a small impact and only at low multipoles. We set the effective sound speed for the perturbations to unity in CAMB, the value for a scalar field.

The marginalized one-dimensional distributions for various data combinations are presented in Figure 9. We find from CMB data alone $w = -0.86^{+0.35}_{-0.36}$. The addition of the LSS data, applying the conservative uniform flat prior on b_g^2 to the galaxy bias factor, yields a median value of $w = -0.64^{+0.15}_{-0.18}$. This result is highly sensitive to our choice of prior on b_g^2. The uniform flat prior on b_g^2 gives a relatively high best-fit bias value of $b_g = 1.3$. Applying a more restrictive Gaussian prior to b_g^2 gives $w = -0.94^{+0.13}_{-0.16}$, with $b_g = 1.0 \pm 0.10$, and $w = -0.74^{+0.13}_{-0.17}$, with $b_g = 1.0 \pm 0.50$. We explore the effect of adding the SNe Ia data, which significantly improves the constraint on w, yielding $w = -0.94^{+0.093}_{-0.097}$, with the flat prior on b_g^2. Results for the CMBall+B03 data set and the CMBall+B03+LSS+SNe Ia data set are given in Table 5.

Figure 10 illustrates the degeneracy in the Ω_m-w plane that cannot be broken by CMB data alone and is only weakly broken with the addition of the LSS data (flat prior on b_g^2). Application of a more restrictive Gaussian prior to b_g^2 for the LSS data or addition of the SNe Ia data breaks the degeneracy.

5. SUBDOMINANT ISOCURVATURE MODEL

CMB anisotropies provide a powerful probe of the nature of early universe perturbations. However, almost any TT power spectrum shape can be fit rather well by using contrived combinations of initial perturbations, for example, by adding structure to the primordial power spectrum and/or by adding isocurvature
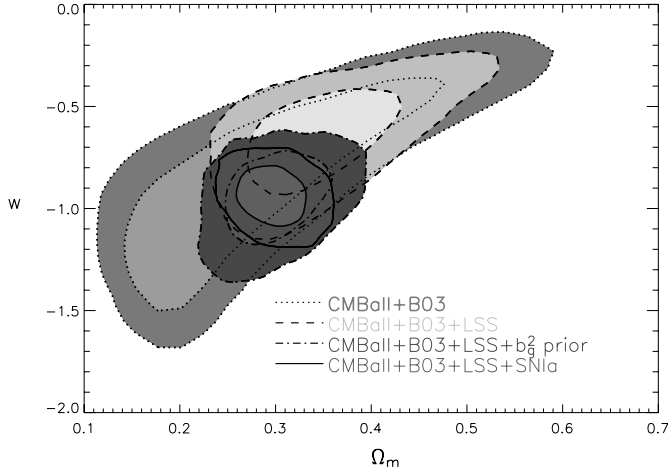
Fig. 10.—Constraints on w vs. Ω_m for a flat ΛCDM model that allows the dark energy equation-of-state parameter, w, to differ from -1. Inner contours represent 68% likelihood regions, and outer contours represent 95% likelihood regions. A more stringent Gaussian b_g^2 prior (with $b_g = 1\% \pm 10\%$) or the addition of SNe Ia data is required to break the strong geometric degeneracy. [*See the electronic edition of the Journal for a color version of this figure.*]

TABLE 6

Marginalized Parameter Constraints for a Model That Includes Both (Dominant) Adiabatic and (Subdominant) Isocurvature Modes

	CMBALL+B03+*HST*		
Parameter (1)	Baseline (2)	Adiabatic+Iso. (3)	Adiabatic+White Iso. (4)
$\Omega_b h^2$	$0.0229^{+0.0011}_{-0.0009}$	$0.0246^{+0.0016}_{-0.0013}$	$0.0234^{+0.0013}_{-0.0010}$
$\Omega_c h^2$	$0.108^{+0.008}_{-0.009}$	0.103 ± 0.009	$0.107^{+0.008}_{-0.009}$
θ	1.045 ± 0.004	$1.051^{+0.006}_{-0.005}$	$1.046^{+0.005}_{-0.004}$
τ	$0.142^{+0.077}_{-0.058}$	$0.156^{+0.078}_{-0.062}$	$0.149^{+0.079}_{-0.063}$
n_s	$0.96^{+0.03}_{-0.02}$	$1.00^{+0.05}_{-0.04}$	$0.96^{+0.03}_{-0.02}$
R_1	...	<0.28	...
R_2	...	<2.3	<3.0
$n_{\rm iso}$	...	$0.99^{+0.63}_{-0.46}$	3.0 (fixed)
$\ln(10^{10} A_s)$	$3.1^{+0.2}_{-0.1}$	3.1 ± 0.1	$3.1^{+0.2}_{-0.1}$
Ω_Λ	0.76 ± 0.04	0.80 ± 0.04	0.77 ± 0.04
Age (Gyr)..........	13.5 ± 0.2	13.2 ± 0.3	13.4 ± 0.2
Ω_m	0.24 ± 0.04	0.20 ± 0.04	0.23 ± 0.04
$z_{\rm re}$	$15.4^{+4.7}_{-4.5}$	15.5 ± 4.4	$15.7^{+4.7}_{-4.8}$
H_0	$73.9^{+4.5}_{-3.5}$	$79.8^{+6.1}_{-5.0}$	$75.5^{+4.8}_{-3.8}$

Notes.—Parameter uncertainties represent the 68% confidence interval. Upper bounds are 95% confidence limits. The flat weak priors are imposed on the base six parameters are as outlined in Table 3. The CMBall data set is defined in Table 2. We include the baseline model result (with the more stringent *HST* prior) for comparison. We consider two parameterizations for the isocurvature model. For the first (col. [2]) we add two parameters to our basic six: $R_2 \equiv \mathcal{P}_{\rm iso}(k_2)/\mathcal{P}_s(k_2)$, with pivot scale $k_2 = 0.05$ Mpc^{-1}, and $R_1 \equiv \mathcal{P}_{\rm iso}(k_1)/\mathcal{P}_s(k_1)$, with $k_1 = 0.005$ Mpc^{-1}. We impose the priors $0 < R_1 < 20$ and $0 < R_2 < 100$. For this case the isocurvature spectral index, $n_{\rm iso}$, is a derived parameter. We also consider the "white isocurvature" case (col. [3]), in which we fix $n_{\rm iso} = 3$ and allow the amplitude ratio $R_2 \equiv (A_{\rm iso}/A_s)$ to lie anywhere between 0 and 100.

modes (which come in many varieties). With full freedom, determination of the basic cosmic parameters suffers because of high correlation with these extra degrees of freedom. These degeneracies are broken by the addition of polarization data, because of the pattern differences of the peaks and troughs between EE, TE, and TT power spectra. In particular the intensity and polarization power spectra for isocurvature modes have the peaks out of phase with those from adiabatic modes (see, e.g., Bond & Efstathiou 1987; Hu et al. 1997). A mix of isocurvature and adiabatic modes can be designed to give acceptable fits to the CMB intensity power spectra (e.g., Bucher et al. 2004; Kurki-Suonio et al. 2005), and the polarization data from B03, as well from DASI, CAPMAP, and CBI, are not yet at the point to clearly distinguish among these more complex models.

To illustrate the constraints that can be determined from the current CMB data, we consider here a simple hybrid case consisting of our basic adiabatic mode model with constant spectral index and a single cold dark matter (CDM) isocurvature mode with its own constant primordial spectral index $n_{\rm iso}$, with no correlation between the two. This adds another two parameters to our basic six, $n_{\rm iso}$ and an amplitude ratio $R_2 \equiv (A_{\rm iso}/A_s)$. We assume the isocurvature perturbations are Gaussian-distributed as we have done for the adiabatic modes. Results are shown in Table 6 for the CMBall+B03+*HST* data combination. Aside from the more stringent *HST* data prior on H_0, all priors on the six base parameters are as outlined in Table 3. Although results indicate that there is no evidence for the presence of an isocurvature mode, the upper limits still allow for a subdominant component.

We now expand on the theoretical framework. Isocurvature modes may arise in two (or more) field models of inflation, and, although certainly not a natural prediction, they have reasonably good physical motivation. Isocurvature modes could also be generated after inflation ended. An ingredient needed for isocurvature modes to have an observable impact on the CMB is that they are associated with a component of significant mass-energy. If the dark matter is cold and of one type, there are two distinct matter isocurvature modes, the baryon and CDM modes, involving primordial fluctuations in the entropy per baryon or the entropy per CDM particle. The classic example of a CDM

possibility is the isocurvature axion mode. It turns out that the isocurvature CDM and baryon modes actually have almost identical signatures in the CMB (Gordon & Lewis 2003), and hence cannot be constrained separately. In this paper we choose to constrain only the CDM isocurvature mode. There are other possibilities for isocurvature modes that we do not explore here.[24]

It is a straightforward modification of CosmoMC to include an additional isocurvature component in the MCMC chains, which uses CAMB to compute the isocurvature power spectra. Instead of using $n_{\rm iso}$ as a basic parameter, we use two amplitude ratios for the two parameters that characterize our CDM isocurvature mode, following a suggestion of Kurki-Suonio et al. (2005):

$$R_2 \equiv \frac{\mathcal{P}_{\rm iso}(k_2)}{\mathcal{P}_s(k_2)}, \quad k_2 = 0.05 \text{ Mpc}^{-1},$$

$$R_1 \equiv \frac{\mathcal{P}_{\rm iso}(k_1)}{\mathcal{P}_s(k_1)}, \quad k_1 = 0.005 \text{ Mpc}^{-1}. \quad (5)$$

[24] One set involves neutrinos and photons compensating each other (Bucher et al. 2000; Rebhan & Schwarz 1994; Lewis 2004), but these must be produced after neutrino decoupling and so seem quite unlikely. Much better motivated are isocurvature modes associated with defects such as cosmic strings created in early universe phase transitions, which would contribute to a subdominant mass-energy content in the present epoch. Cosmic-defect-induced perturbations are greatly modified from their largely uncorrelated initial state through gravity wave emission and have distinctively non-Gaussian features. By themselves they cannot explain the CMB data since the peaks and troughs are difficult to mimic, but they could be a subdominant component that future CMB data should be able to constrain.

Here $\mathcal{P}_s(k)$ is the power in the primordial curvature perturbation, and $\mathcal{P}_{\mathrm{iso}}(k)$ is the power in the primordial CDM-photon entropy perturbation. The k_2 scale corresponds to $l \sim 700$ and k_1 to $l \sim 70$. We adopt a uniform prior probability over the range 0–20 for R_1 and over the range 0–100 for R_2. The isocurvature spectral index n_{iso}, defined by $\mathcal{P}_{\mathrm{iso}}(k) \propto k^{n_{\mathrm{iso}}}$, is now a derived parameter, expressible in terms of R_1, R_2 and the adiabatic spectral index n_s, defined by $\mathcal{P}_s(k) \propto k^{n_s-1}$,

$$n_{\mathrm{iso}} = n_s - 1 + \frac{\ln(R_2/R_1)}{\ln(k_2/k_1)}. \qquad (6)$$

Two interesting limiting cases are the scale-invariant $n_{\mathrm{iso}} = 0$ spectrum with high spatial correlation and the $n_{\mathrm{iso}} = 3$ "isocurvature seed" white-noise spectrum with no spatial correlation.[25]

The limits shown in Table 6 demonstrate that the large-scale R_1, dominated by the *WMAP* data, is much better constrained at <0.3 than the small-scale $R_2 < 2.3$, which B03 probes. This translates into a preference for steeper n_{iso} than the scale-invariant value. Since for neither is there an indication of a nonzero value, just upper limits, the results are sensitive to the prior probabilities we assign them. Our choice of uniform prior for R_1 and R_2 is conservative in that the upper limits decrease with other choices, e.g., one uniform in $\ln(R_i)$ (a noninformative prior) or one uniform in n_{iso} and R_2. The conservative choice actually downgrades the probability of steep n_{iso}. (The B03 pol data by itself only limit $R_1 < 17$ and $R_2 < 22$; the full B03 data give $R_1 < 1.8$ and $R_2 < 5.3$.) Further constraints on isocurvature modes arise from LSS since the shape of the isocurvature matter power spectrum differs in significant ways from the adiabatic one, but we do not consider those here.

The strongest constraints come from the low-l part of the spectrum.[26] However, spectra that are significantly steeper than inflation-motivated, nearly scale-invariant ones are still allowed by the data. To focus attention on the role played by the new, high-l B03 results, we now fix n_{iso} at 3, the white-noise "seed" spectrum, the limiting case in which the isocurvature perturbations when created were uncorrelated spatially. The large angular scales are highly suppressed, and the isocurvature peaks and troughs emerge looking somewhat like an l-shifted version of the adiabatic spectrum. The two spectra then test at what level interleaved isocurvature peaks are allowed by the CMB data. Results are shown in Table 6. To relate the $R_2 < 3.0$ limit to a more intuitive expression of what the CMBall+B03+*HST* data set allows, we note that over a band power in l from 75 to 1400, $\mathcal{C}_B^{\mathrm{TT(iso)}}/\mathcal{C}_B^{\mathrm{TT}(s)} \sim 0.005 R_2$; hence, the upper limit corresponds to an allowed CMB contamination of this subdominant component of TT of only a few percent. Over a band power in l from 150 to 1000, we find $\mathcal{C}_B^{\mathrm{EE(iso)}}/\mathcal{C}_B^{\mathrm{EE}(s)} \sim 0.008 R_2$ for the allowed EE isocurvature

band power contamination. B03 pol gives $R_2 < 58$. The full B03 data set including TT gives $R_2 < 9.5$.[27] Since the isocurvature models adopted for these tests are not especially well-motivated physically, we have also chosen not to apply the LSS prior to our results.

The $n_{\mathrm{iso}} = 3, 2$ illustration allows us to conclude that even with the errors on the EE and TE data, there is evidence against the isocurvature-shifted pattern over the adiabatic pattern and only restricted room for an interleaved peak pattern, at a level below 50%. This test differs from the adiabatic-only peak/trough pattern shift using B03 pol (Fig. 3) since there are no interleaved peaks and troughs in that case. Examination of the CAMB models obtained from the marginalized constraints in Table 6 reveals that the parameters chosen by CosmoMC adjust to make the adiabatic $\mathcal{C}_l^s$ pattern compensate for the isocurvature $\mathcal{C}_l^{\mathrm{iso}}$ contamination.

6. CONCLUSIONS

The B03 data set does well at constraining the cosmological parameters of the standard ΛCDM model. The results are in good agreement with those derived from other CMB experiments, as is evident in Table 4. The parameter constraints derived from the B03 data set in combination with the *WMAP* data are highly competitive with those from the CMBall data set.

We have applied the Slosar-Seljak modification to the *WMAP* data, which has the general effect of broadening slightly the *WMAP* one-dimensional likelihood curves with the largest impacts on the (*WMAP* alone) median values of τ ($\sim 0.3\,\sigma$ increase) and Ω_m ($\sim 0.6\,\sigma$ decrease) for the baseline model and n_{run} ($\sim 0.5\,\sigma$ increase) for the baseline+running index model. Our graphical representation of the standard model parameters in Figure 2 illustrates the impact of the addition of the LSS data, which shifts the median values very little. Figure 2 shows the best estimates for the parameters of the ΛCDM model from current CMB and LSS redshift survey data.

Our analysis of five extensions to the standard model is summarized in Table 5. Intriguingly we found two cases, the running index and neutrino fraction, in which the addition of data from higher multipole CMB experiments drove median values away from the conventional value. The evidence for a running index, however, is slight ($<2\,\sigma$). Our neutrino mass limit (assuming three species of nearly degenerate mass) from CMB data alone is $m_\nu < 1.0$ eV and from the combined CMB and LSS data set is $m_\nu < 0.40$ eV, with no b_g prior, and $m_\nu < 0.16$ eV, with $b_g = 1.0 \pm 0.10$.

We have explored the sensitivity of our CMBall+B03+LSS results to the prior imposed on the galaxy bias factor b_g and have found that only the neutrino mass results (above) and dark energy equation-of-state results are significantly impacted. For the dark energy equation of state we find that applying a more restrictive Gaussian prior to b_g^2 gives $w = -0.94^{+0.13}_{-0.16}$, with $b_g = 1.0 \pm 0.10$. Without any b_g constraint we find $w = -0.64^{+0.15}_{-0.18}$. However, addition of the SNe Ia data, with the flat prior on b_g^2, yields $w = -0.94^{+0.093}_{-0.097}$. The results are consistent with the dark energy being the cosmological constant.

While the polarization data are not yet at the level of accuracy of the intensity data, cross-checks of best-fit parameters from the B03 pol data and B03 TT data indicate consistent results. The

---

[25] Such a spectrum is so steep that it must be regulated by a cutoff at high $k \gg k_2$. Physically this is typically the scale of the horizon when they are generated, but it is constrained by small-scale structure information such as the allowed epoch of first star formation, which cannot be too early or else τ could be far too large. We do not add this cutoff to our study since the CMB has a larger natural damping scale. A traditional seed case that has been considered is primordial black hole production.

[26] This is largely because of the isocurvature effect (Efstathiou & Bond 1986): to have no overall energy density perturbation on large scales, the entropy perturbation is carried almost entirely by the CDM and baryons, but when the equation of state changes from radiation to matter dominance the photons carry the perturbation. The result is a rather dramatic amplification in the power over the Sachs-Wolfe power familiar in the adiabatic case by 36. This is why the nearly scale-invariant case for isocurvature alone has been ruled out for so long from CMB data, so there was only room for it appearing at a subdominant level.

[27] The $n_{\mathrm{iso}} = 2$ case mimics even more the peak/trough patterns in $\mathcal{C}_l$ except for the shift, so we tested that case as well. CMBall+B03+*HST* gives $R_2 < 2.7$; B03 alone, but with TT, gives $R_2 < 6.8$; and B03 pol gives $R_2 < 41$. Translation to the allowed contamination is done with the band power ratios $\mathcal{C}_B^{\mathrm{TT(iso)}}/\mathcal{C}_B^{\mathrm{TT}(s)} \sim 0.007 R_2$, $\mathcal{C}_B^{\mathrm{EE(iso)}}/\mathcal{C}_B^{\mathrm{EE}(s)} \sim 0.009 R_2$.

consistency of the shape parameter θ determined from B03 pol and from B03 TT demonstrates that the peak and trough positions forecast by the spectra are in robust agreement. Isocurvature modes are beginning to be constrained by the current CMB polarization data, and our upper limits and phenomenological discussion represent a good starting point for future analysis of these more complex models. The CMB polarization data are emerging but are not yet driving parameter determination. We look forward to future higher precision data in which polarization data will play a larger role.

REFERENCES

Ahmad, Q. R., et al. 2002, Phys. Rev. Lett., 89, 011301
Aliani, P., Antonelli, V., Picariello, M., & Torrente-Lujan, E. 2003, preprint (hep-ph/0309156)
Bond, J. R., Contaldi, C. R., Lewis, A. M., & Pogosyan, D. 2004, Int. J. Theor. Phys., 43, 599
Bond, J. R., Contaldi, C. R., & Pogosyan, D. 2003, Philos. Trans. R. Soc. London A, 361, 2435
Bond, J. R., & Efstathiou, G. 1987, MNRAS, 226, 655
Bond, J. R., Efstathiou, G., & Tegmark, M. 1997, MNRAS, 291, L33
Bond, J. R., Jaffe, A. H., & Knox, L. E. 2000, ApJ, 533, 19
Bond, J. R., et al. 2005, ApJ, 626, 12
Bucher, M., Dunkley, J., Ferreira, P. G., Moodley, K., & Skordis, C. 2004, Phys. Rev. Lett., 93, 081301
Bucher, M., Moodley, K., & Turok, N. 2000, Phys. Rev. D, 62, 083508
Chon, G., Challinor, A., Prunet, S., Hivon, E., & Szapudi, I. 2004, MNRAS, 350, 914
Christensen, N., Meyer, R., Knox, L., & Luey, B. 2001, Classical Quantum Gravity, 18, 2677
Cole, S., et al. 2005, MNRAS, 362, 505
Contaldi, C. R., Hoekstra, H., & Lewis, A. 2003, Phys. Rev. Lett., 90, 221303
de Bernardis, P., et al. 2000, Nature, 404, 955
Dickinson, C., et al. 2004, MNRAS, 353, 732
Dore, O., Holder, G. P., & Loeb, A. 2004, ApJ, 612, 81
Efstathiou, G., & Bond, J. R. 1986, MNRAS, 218, 103
Eidelman, S., et al. 2004, Phys. Lett. B, 592, 1
Eisenstein, D. J., et al. 2005, ApJ, 633, 560
Freedman, W. L., et al. 2001, ApJ, 553, 47
Frigo, M., & Johnson, S. G. 2005, Proc. IEEE, 93, 216
Gordon, C., & Lewis, A. 2003, Phys. Rev. D, 67, 123513
Gorski, K. M., et al. 2005, ApJ, 622, 759
Halverson, N. W., et al. 2002, ApJ, 568, 38
Hanany, S., et al. 2000, ApJ, 545, L5
Hedman, M. M., et al. 2002, ApJ, 573, L73
Hinshaw, G., et al. 2003, ApJS, 148, 135
Hivon, E., et al. 2002, ApJ, 567, 2
Hu, W., Sugiyama, N., & Silk, J. 1997, Nature, 386, 37
Huey, G., Wang, L., Dave, R., Caldwell, R. R., & Steinhardt, P. J. 1999, Phys. Rev. D, 59, 063005

Jones, W. C., et al. 2006a, ApJ, 647, 823
———. 2006b, A&A, submitted (astro-ph/0606606)
Kogut, A., et al. 2003, ApJS, 148, 161
Kosowsky, A., Milosavljevic, M., & Jimenez, R. 2002, Phys. Rev. D., 66, 063007
Kosowsky, A., & Turner, M. S. 1995, Phys. Rev. D, 52, 1739
Kovac, J., et al. 2002, Nature, 420, 772
Kuo, C. L. et al. 2004, ApJ, 600, 32
Kurki-Suonio, H., Muhonen, V., & Väliviita, J. 2005, Phys. Rev. D, 71, 063005
Lange, A. E., et al. 2001, Phys. Rev. D, 63, 042001
Lewis, A. 2004, Phys. Rev. D, 70, 043518
Lewis, A., & Bridle, S. 2002, Phys. Rev. D, 66, 103511
Lewis, A., Challinor, A., & Lasenby, A. 2000, ApJ, 538, 473
Masi, S., et al. 2005, preprint (astro-ph/0507509)
McDonald, P., et al. 2006, ApJS, 163, 80
Montroy, T., et al. 2006, ApJ, 647, 813
Neal, R. M. 1993, preprint, http://www.cs.toronto.edu/~radford/review.abstract.html
Netterfield, C. B., et al. 2002, ApJ, 571, 604
Percival, W. J., et al. 2001, MNRAS, 327, 1297
Piacentini, F., et al. 2006, ApJ, 647, 833
Ratra, B., & Peebles, P. J. E. 1988, Phys. Rev. D, 37, 3406
Readhead, A. C. S., et al. 2004a, ApJ, 609, 498
———. 2004b, Science, 306, 836
Rebhan, A. K., & Schwarz, D. J. 1994, Phys. Rev. D, 50, 2541
Riess, A. G., et al. 2004, ApJ, 607, 665
Ruhl, J. E., et al. 2003, ApJ, 599, 786
Seljak, U., & Zaldarriaga, M. 1996, ApJ, 469, 437
Seljak, U., et al. 2004, Phys. Rev. D, 71, 103515
———. 2005, Phys. Rev. D, 71, 043511
Slosar, A., Seljak, U., & Makarov, A. 2004, Phys. Rev. D, 69, 123003
Spergel, D. N., et al. 2003, ApJS, 148, 175
Tegmark, M., et al. 2004, ApJ, 606, 702
Toshito, T., et al. 2001, preprint (hep-ex/0105023)
Tristram, M., et al. 2005, A&A, 436, 785
Verde, L., et al. 2002, MNRAS, 335, 432
———. 2003, ApJS, 148, 195